Available online at www.sciencedirect.com
ScienceDirect
Journal of the European Ceramic Society 27 (2007) 4613–4621
www.elsevier.com/locate/jeurceramsoc

Creep behaviour of alumina–mullite–zirconia nanocomposites obtained by a colloidal processing route

R. Torrecillas *, M. Schehl, L.A. Díaz

Nanostructured Materials Group, Chemistry of Materials Department, Instituto Nacional del Carbón-CSIC, Francisco Pintado Fe 26, 330011 Oviedo, Spain

Received 10 April 2007; accepted 5 May 2007
Available online 23 July 2007

Abstract

The high-temperature creep behaviour of high-purity alumina (A) and an alumina–mullite–zirconia nanocomposite (AZS) has been studied. The alumina–mullite–zirconia nanocomposite was prepared by using a colloidal processing route (powder–alkoxide mixtures). Creep tests were carried out in air in a 4-point-bending-fixture from 1200 to 1400 °C under constant stresses ranging from 30 to 220 MPa. Creep parameters (stress exponent n and activation energy Q) were correlated with microstructural features in order to determine the dominant creep mechanisms for both materials. The slow crack growth region (SCG), given by pairs of critical stress and the corresponding critical strain rate at the temperatures 1200, 1300 and 1400 °C of both materials was studied.

It was found that the creep rate of AZS was two orders of magnitude lower than the creep rate of undoped alumina A. The dominant creep mechanism of A is assumed to be a combination of grain boundary and lattice diffusion controlled creep. The creep mechanism for AZS is different and depends on the temperature. It is supposed that lattice diffusion controlled creep (Nabarro–Herring) is the dominant creep mechanism at 1200 °C, whereas at 1300 °C it is supposed to be grain boundary sliding accommodated by grain boundary diffusion. Comparing the slow crack growth region of both materials, a dramatic improvement was observed. The slow crack growth region of alumina is shifted nearly twice concerning the applied stresses for AZS at the temperatures 1200, 1300 and 1400 °C.

Keywords: Creep; Nanocomposites; Al_2O_3; Colloidal processing; Grain boundary

1. Introduction

At present, alumina is the most common ceramic material for industrial applications. It has quite good bending strength, but fracture toughness is quite low (4–5 to 5 MPa $m^{1/2}$ for >99% purity). High-purity alumina presents a fair creep resistance, depending on the impurity content present in the starting powders as well as the cleanness of the atmosphere during sintering. Taking into account that the material is quite cheap, it can be concluded that all efforts dealing with an improvement of fracture toughness and creep resistance should have an important technological impact for the potential uses of alumina. For these reasons researchers investigated in recent years the addition of dopants in order to get better densification behaviour, higher densities, better microstructures and better creep behaviour.[1,2] Most of the intentionally added dopants present a low limit of solubility in alumina and thus are segregated to grain boundaries. At higher concentrations, some of them form secondary phases at grain boundaries (crystalline or amorphous) leading to important modifications in the microstructure and thus modifying the whole properties of alumina. Several approaches can be followed to increase the creep rate of alumina. For example, the formation of secondary phases which form a strong interface with alumina could drastically reduce the creep rate at high temperatures.[2] Also, the formation of phases with different thermal expansion coefficients could introduce thermal stresses at grain boundaries clearly modifying the crack propagation behaviour. Thus, the tailoring of microstructures in order to enhance creep behaviour of alumina nanocomposites over a range of temperatures should be possible.

There was not much research carried out during the last 10 years concerning the creep behaviour of composites in the

* Corresponding author.
E-mail address: rtorre@incar.csic.es (R. Torrecillas).

0955-2219/$ – see front matter © 2007 Elsevier Ltd. All rights reserved.
doi:10.1016/j.jeurceramsoc.2007.05.001

system alumina–mullite–zirconia. Torrecillas et al.[3] produced mullite–zirconia–alumina composites by reaction sintering of alumina and zircon powders. The obtained composite presents mullite as the matrix phase (55 wt%) and zirconia (31.85 wt%) and alumina (13.15 wt%) at grain boundaries. These researchers examined the creep behaviour with an applied stress of 100 MPa at the temperature range 1200–1400 °C and observed a very low creep rate (10^{-10} s^{-1}) at the temperature interval 1200–1300 °C. Jang et al.[4,5] used a new colloidal processing route to prepare a dense 50 wt% alumina–30 wt% mullite–20 wt% zirconia composite. They investigated phase formation, microstructural development and toughening mechanisms operating on this composite. Mazzei and Rodrigues[6] and Mazzei et al.[7] produced alumina–mullite–zirconia composites by reaction sintering of zircon and alumina powders with the following alumina percentages after sintering: 89.47 wt% (comp. 1), 79.07 wt% (comp. 2), 68.85 wt% (comp. 3), 58.79 wt% (comp. 4) and 48.89 wt% (comp. 5), having in all cases alumina as the matrix phase. They studied the microstructure, the mechanical properties and the *R*-curve behaviour of these five composites.

Li et al.[8] co-doped ultra-high-purity α-alumina powder (AKP-53, Sumitomo, Japan) with different dopants such as 100 ppm Nd, 100 ppm Zr, 100 ppm Nd/100 ppm Zr, 350 ppm Nd/100 ppm Zr, 1000 ppm Nd/100 ppm Zr and 1000 ppm Sc/100 ppm Zr. The quantity of ZrO_2 was always 100 ppm. The researchers studied the influence of doping on the flow stress, creep rate, stress exponent and activation energy. A study of the slow crack region (SCG) given by pairs of critical stress and the corresponding critical strain rate at different temperatures was undertaken for mullite by Torrecillas et al.[9] Similar studies for alumina and alumina–mullite–zirconia nanocomposites have not yet been realised.

Lowering the creep rate of alumina requires a very homogenous microstructure. For secondary phase precipitates only intergranular and not intragranular particles should be present in the microstructure. Additionally, homogenous size distributions are required for both alumina and secondary phase particles. In order to reach these objectives, special care has to be taken during the processing step.

In the present study, the creep behaviour of ultra high-purity alumina (Condea HPA0,5) (A) and ultra-high-purity alumina doped with a mixture of zirconium *n*-propoxide and tetraethyl orthosilicate (TEOS) in the stoichiometrie of zircon (AZS) is compared. AZS was prepared by using a colloidal processing route using a powder–alkoxide mixture.[1] The slow crack growth region for both materials (A and AZS) was also studied.

2. Experimental procedure

2.1. Materials

A commercial high-purity α-alumina (Al_2O_3) powder (HPA0,5, Condea, Hamburg, Germany) with $d_{50} = 0.46$ μm, a specific surface area of 9.9 m^2/g and 99.99% purity was used as starting material. The chemical analysis of this high-purity alumina powder is shown in Table 1. This alumina powder was sieved under 45 μm, cold isostatic pressed (C.I.P.) at 200 MPa and finally sintered in air at 1600 °C for 2 h. This sample was called A. The grain boundary modification was achieved by the dropwise addition, to an alumina powder dispersed in anhydrous 99.97% ethanol, of a mixture of zirconium IV-propoxide (70% solution in 1-propanol) (Sigma–Aldrich, Spain) and tetraethyl orthosilicate TEOS 98% (Sigma–Aldrich) in the stoichiometrie of zircon. The slurry was first dried under magnetic stirring at 70 °C and subsequently in air at 120 °C for 24 h in order to eliminate the rest of the alcohols. The dried powder was subsequently crushed to remove agglomerates resulting from the drying process. The powder was thermally treated at 850 °C for 2 h in order to remove organic residuals and subsequently attrition milled with zirconia balls for 30 min. After drying, the powder was sieved under 45 μm. The obtained powder was cold isostatic pressed at 200 MPa and sintered in air at 1600 °C for 2 h. This sample was called AZS.

Table 1
Chemical analysis of α-Al_2O_3 powder (Condea HPA0,5)

Trace impurities (ppm)														
Na	Si	Fe	Ca	Mg	Ga	Cr	Ni	Ti	Mn	Cu	Mo	Li	Zn	Zr
19	25	14	4	4	<4	3	<1	8	1	<1	<4	<1	1	4

2.2. Characterisation techniques

Creep tests were carried out in air in a 4-point-bending-fixture at temperatures ranging from 1200 to 1400 °C under stresses from 30 to 220 MPa using a Instron 8562 testing machine. The heating rate of the furnace was 300 °C/h in order to avoid significant thermal gradients and thus thermal instabilities. In order to obtain dimensional stability of all parts of the testing machine, the holding time at the test temperature was 1 h. At the corresponding temperature, a constant load *P* was applied immediately and the specimen deflection (on the tensile face) at the centre of the sample and the applied load were recorded as function of time.

The specimens were parallelepipeds with the following dimensions: *b* (sample width) 4 mm, *w* (sample height) 3 mm and *l* (sample length) 35 mm. The tensile face of all the specimens was polished with diamond paste down to 3 μm and the edges were chamfered (about 45°) in order to avoid influences of microcrack formation on the creep behaviour.

A 4-point-bending-fixture of alumina with an outer span of 28 mm and an inner span of 14 mm was used and the flexural stress on the tensile face of the specimen was calculated by the following expression:

$$\sigma = \frac{3P(L - L')}{2bw^2}, \quad (1)$$

where *P* is the applied load, *L* the outer span, *L′* the inner span, *b* the sample width and *w* is the sample height.

Hollenberg et al.[10] showed that the creep strain ε can be calculated from the deflection *y* at the centre of the specimen if there is no major cracking in the specimen and the deflection *y*

is small compared to the inner span L':

$$\varepsilon = K(n)y, \tag{2}$$

with

$$K(n) = \frac{2w(n+2)}{(L-L')[L+L'(n+1)]}. \tag{3}$$

The constant $K(n)$, in addition to its dependence on n, is also a function of the spans L and L'. Hollenberg et al.[10] have shown that for (L/L') values close to 2, $K(n)$ is almost insensitive to the n value. So, expression (2) can be used and ε calculated with an approximated value for n. In case of too high divergence between the determined n and the initial supposed n, calculations of ε must be realised again.

For microstructural observations by scanning electron microscopy (SEM), the surfaces of the sintered specimens were polished and thermally etched at 1400 °C/1 h to reveal grain morphologies.

3. Results and discussion

3.1. Microstructure

Fig. 1(a and b) shows the microstructure of the non-deformed samples A and AZS, respectively. Alumina (A) shows a dense and homogenous microstructure with a mean grain size of 5.9 μm. All alumina grains are nearly equiaxed. The sample AZS has a dispersion of secondary phase particles located at alumina grain boundaries and triple points. These secondary phase particles at the alumina grain boundaries are tetragonal zirconia and mullite. All of these tetragonal zirconia and mullite particles are located at alumina grain boundaries or triple points. No intragranular secondary phase particles were found and about 100% of all alumina triple points are occupied, taking into account that the image observed is a section of the composite and as a consequence the triple points observed are not real triple points. The different triple points in this sample can be occupied by zirconia or mullite or zirconia and mullite particles. The distribution of the mullite and zirconia particles throughout the alumina matrix is homogenous, with a mean particle size of 200 nm for the zirconia particles, 600 nm for the mullite particles and 1.9 μm for the alumina particles. Figs. 2(a and b) and 3(a and b) show the fracture surfaces before and after creep measurements for A and AZS, respectively. It is evident that no significant grain growth occurred during creep deformation.

3.2. Creep parameters and slow crack growth

The creep behaviour of A and AZS at 1300 °C is shown in Fig. 4(a and b) in a strain versus time plot. For A the applied stresses range from 30 to 100 MPa, while for AZS nanocomposites they range from 30 to 170 MPa. All creep curves show only the primary creep and steady-state creep region. No tertiary creep region was observed, even in case of broken specimens. Both materials A and AZS reached the steady state at 1300 °C for all applied stresses as it can be observed in Fig. 5(a and b)

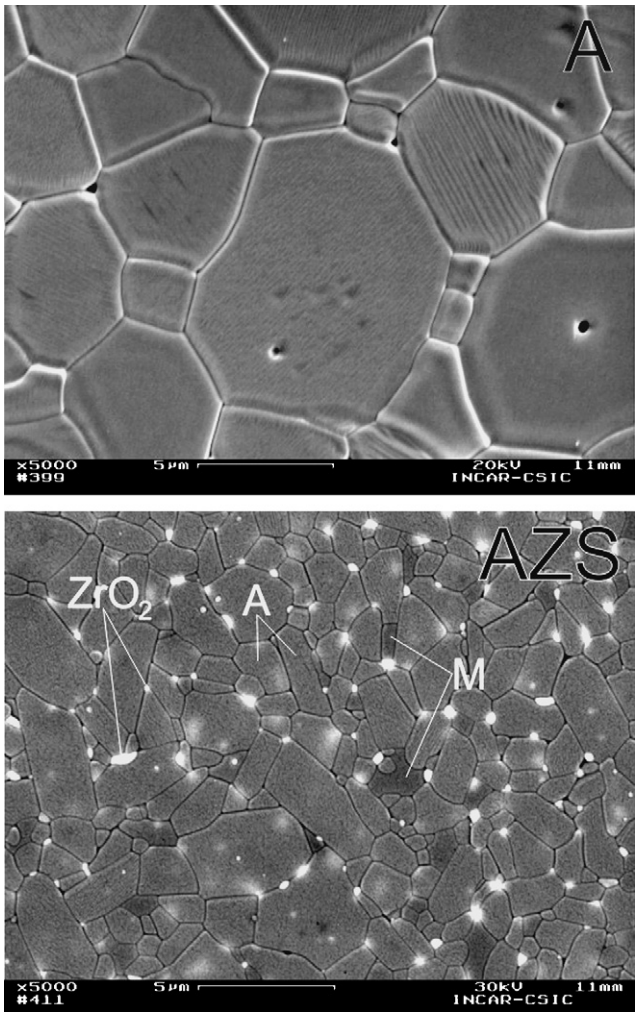

Fig. 1. SEM micrograph of: (a) A and (b) AZS.

in a strain rate versus time plot. Considering the time interval of 0–65 h, there was no specimen fracture observed for A up to an applied stress of 80 MPa, whereas for AZS an applied stress of 150 MPa was possible without fracture of the sample considering the stress interval 0–2.5%. For the applied stress of 150 MPa a time interval could not be applied, because the method for the calculation of the stress is limited, meaning that the deflection of the sample is more than 10% of the inner span of the 4-point-bending-fixture.[10] At 1300 °C fracture occurs with an applied stress of 100 MPa for A, while 170 MPa was necessary for AZS in order to observe the fracture of the specimen by slow crack growth. Fracture of samples A and AZS occurs approximately after 4 h. This similar fracture behaviour for A and AZS at 1300 °C is not observed at 1200 and 1400 °C, meaning that A deforms for a time interval between 2 and 4 h before rupture, while the fracture of AZS occurs at 1200 °C after 36 h, at 1300 °C after 4 h and at 1400 °C after a few minutes.

It is important to point out that with a relatively small quantity of tetragonal zirconia and mullite particles at grain boundaries and triple points, the slow crack growth region of alumina is moved from 80 MPa for A to 150 MPa for AZS, nearly two times of the applied stress.

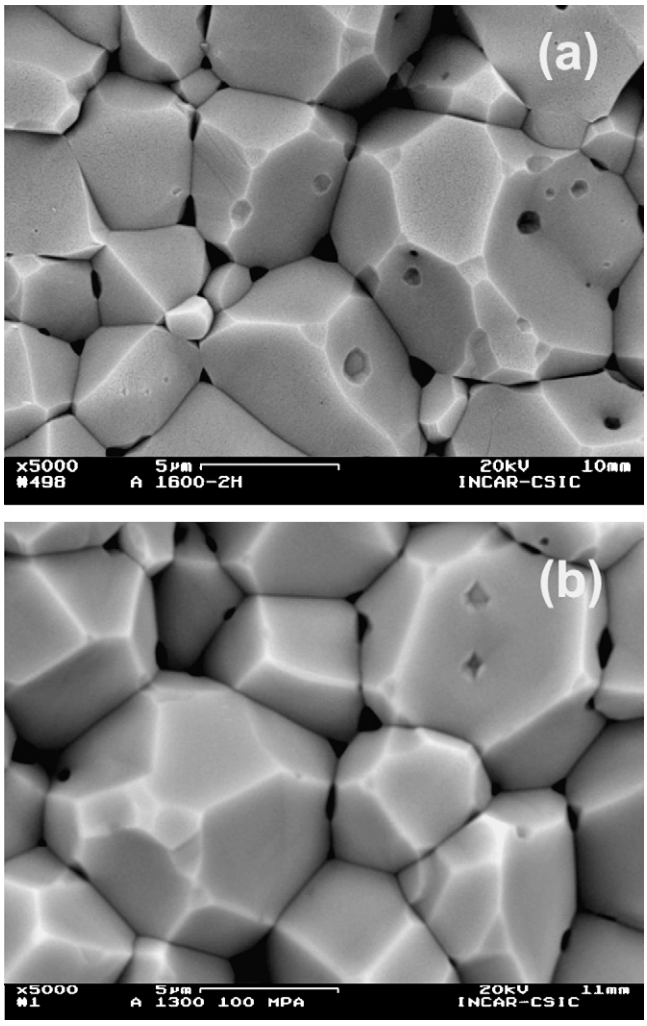

Fig. 2. Fracture surfaces of A before (a) and after (b) creep measurements.

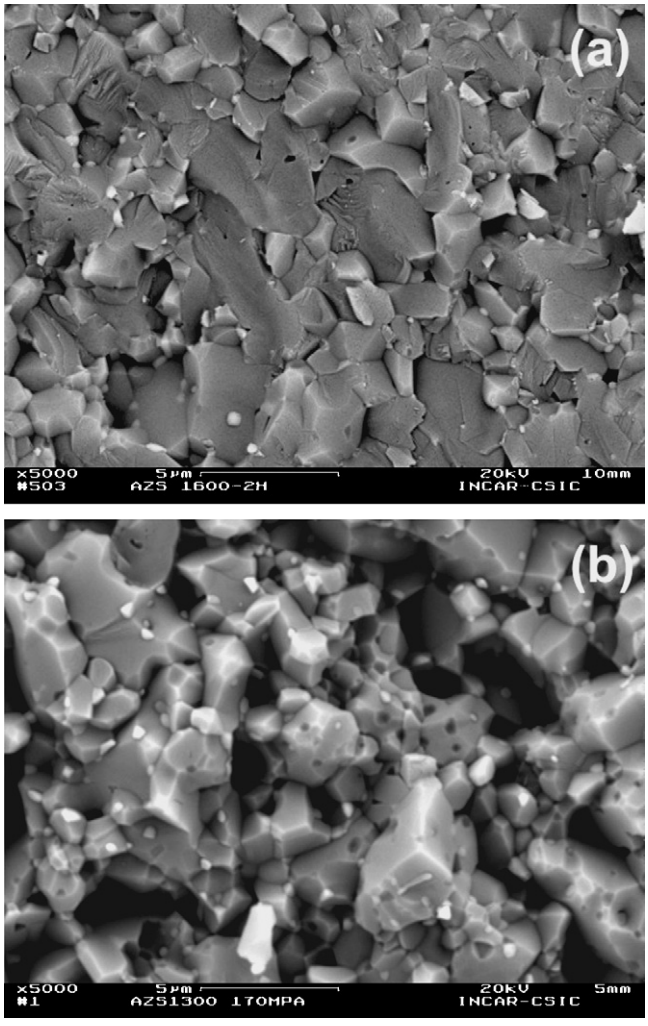

Fig. 3. Fracture surfaces of AZS before (a) and after (b) creep measurements.

The steady-state creep rate $\dot{\varepsilon}$ is expressed by the following equation:

$$\dot{\varepsilon} = A\frac{\sigma^n}{d^p}\exp\left(-\frac{Q}{RT}\right), \quad (4)$$

where A is the material constant, σ the applied stress, n the stress exponent, d the grain size, p the grain size exponent, Q the activation energy for creep, R the gas constant and T is the absolute temperature.

A complete creep behaviour characterisation for A and AZS was realised at the temperature range 1200–1400 °C with different applied stresses in order to determine the stress exponents n for a given temperature and the activation energies Q for a given stress.

Fig. 6 shows the steady-state creep rate as a function of the applied stress in a log–log plot for A and AZS, respectively. The applied stresses were 30–120 MPa for A and 30–220 MPa for AZS at the temperature range 1200–1400 °C. The stress exponents n for A and AZS were determined for the constant temperatures 1200, 1300 and 1400 °C. The stress exponent n for A at 1200 and 1300 °C was nearly the same, being $n = 1.52$ and $n = 1.46$ at 1200 and 1300 °C, respectively. At 1400 °C the stress exponent raises to $n = 1.76$. The sample AZS has a stress exponent of 1.21 at 1200 °C and 1.53 at 1300 °C. At 1400 °C the stress exponent raises to 1.67. Sample A shows only a small difference in their measured n at 1200 and 1300 °C, which can be explained as experimental scatter, whereas AZS has clearly two different stress exponents n at 1200 and 1300 °C, respectively. At 1400 °C the values of n for both materials are raised. In this study, the stress exponent for A is around 1.5 at 1200 and 1300 °C. This value is comparable with stress exponents determined for alumina by other researchers.[8,15–21] For AZS the determined stress exponent is nearly 1.2 at 1200 °C and 1.5 at 1300 °C. On a first view the calculated stress exponent at 1200 °C seems to be rare because other researchers[22,23,28] calculated stress exponents around 2 for alumina doped with different quantities of zirconia. The explanation was found studying the sintering behaviour and the phase evolution during sintering.[1] The differential shrinkage curve of AZS showed a sudden increase at the temperature interval 1580–1630 °C. It is assumed that this is due to the formation of mullite via a dissolution–precipitation mechanism because XRD revealed the formation of mullite at 1550 °C. The formation of mullite through a transitory glassy phase is related with a high volume increase. It is believed that this volume increase

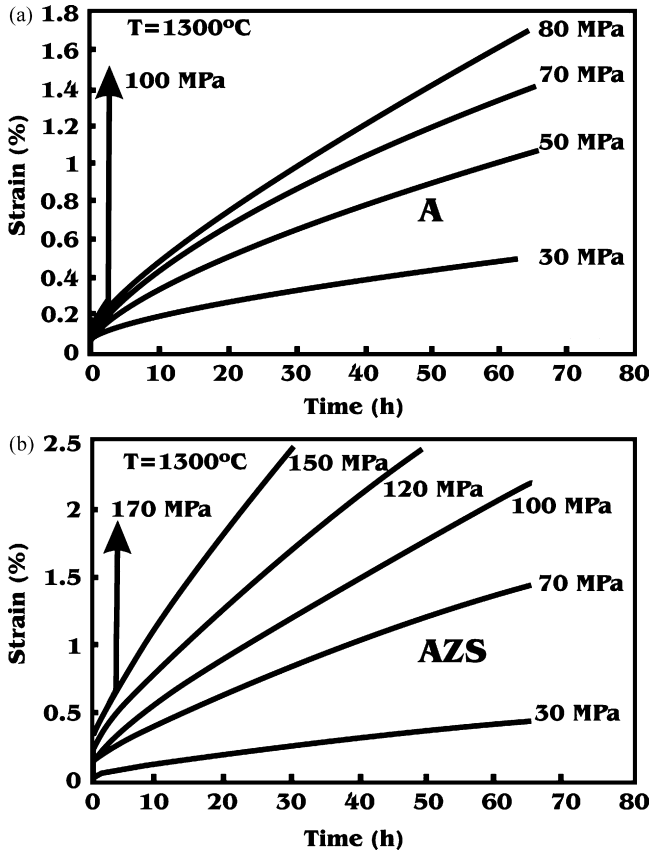

Fig. 4. Creep curves of: (a) A and (b) AZS at 1300 °C.

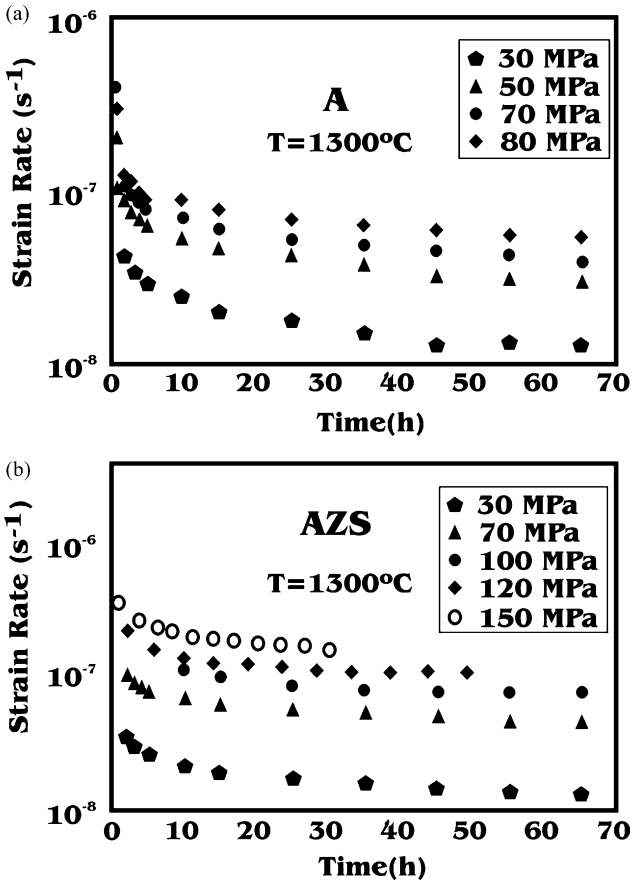

Fig. 5. Strain rate evolution vs. time for: (a) A and (b) AZS at 1300 °C.

due to the formation of mullite introduces residual stresses at alumina grain boundaries. During cooling these residual stresses are maintained and even increased due to the different thermal expansion coefficients of alumina with $\alpha_{Al_2O_3} = 9.0 \times 10^{-6}\,^{\circ}C^{-1}$,[24,25] mullite with $\alpha_{Mullite} = 5.1 \times 10^{-6}\,^{\circ}C^{-1}$[26] and tetragonal zirconia with $\varepsilon_{t\text{-}ZrO_2} = 16 \times 10^{-6}\,^{\circ}C^{-1}$.[27] When heating up to 1200 °C, a part of these residual stresses still exists and thus the stress exponent at 1200 °C is similar to the stress exponent of pure mullite (1.2).[9] Thus, it may be concluded that the small quantity of mullite nanoparticles is controlling the creep behaviour of AZS at 1200 °C and as a consequence lattice diffusion (Nabarro–Herring) is the controlling mechanism in this composite at this temperature. At 1300 °C the residual stresses are removed and an equilibrium between mullite and tetragonal zirconia particles is reached and, as a consequence, the creep behaviours of A and AZS at low stresses are very similar. At 1400 °C the values of n for both materials, A and AZS, are raised. These values are overestimated. This overestimation becomes obvious in Fig. 7(a and b), where the strain rate is represented as a function of time. At 1400 °C and with high-applied stresses the curves are still in the primary creep region, meaning that the steady state is not reached and thus the calculated strain rates cannot be considered as steady-state creep rates.

Fig. 8(a and b) shows the relationship of the steady-state creep rate $\dot{\varepsilon}$ and the reciprocal of the absolute temperature $1/T$ in a $\log \dot{\varepsilon} - 1/T$ plot for A and AZS, respectively. The used stresses for the determination of the activation energies Q were 50 and 70 MPa for A, while for AZS stresses of 70 and 100 MPa were applied. The temperature range was 1200–1400 °C for both materials. For A with an applied stress of 50 MPa the activation energy was 517 kJ/mol, whereas for an applied stress of 70 MPa the calculated activation energy was 527 kJ/mol. AZS has an activation energy Q of 692 kJ/mol for an applied stress of 70 MPa and 736 kJ/mol for an applied stress of 100 MPa.

In Fig. 6 two regions can be clearly discriminated, a region where no specimen fracture occurs for the time interval 0–65 h or stress interval 0–2.5% and the other region where specimen fracture occurs. The latter one is called slow crack growth region.

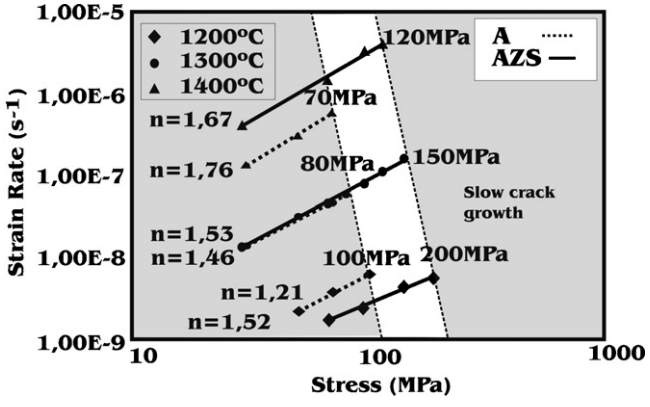

Fig. 6. Steady-state creep rate vs. applied stress for A and AZS.

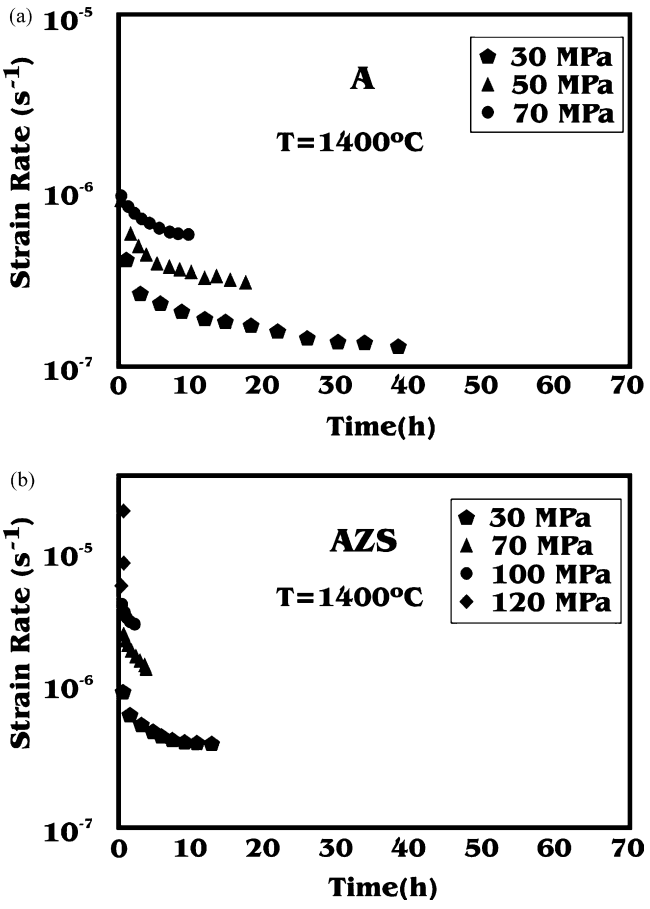

Fig. 7. Strain rate evolution vs. time for: (a) A and (b) AZS at 1400 °C.

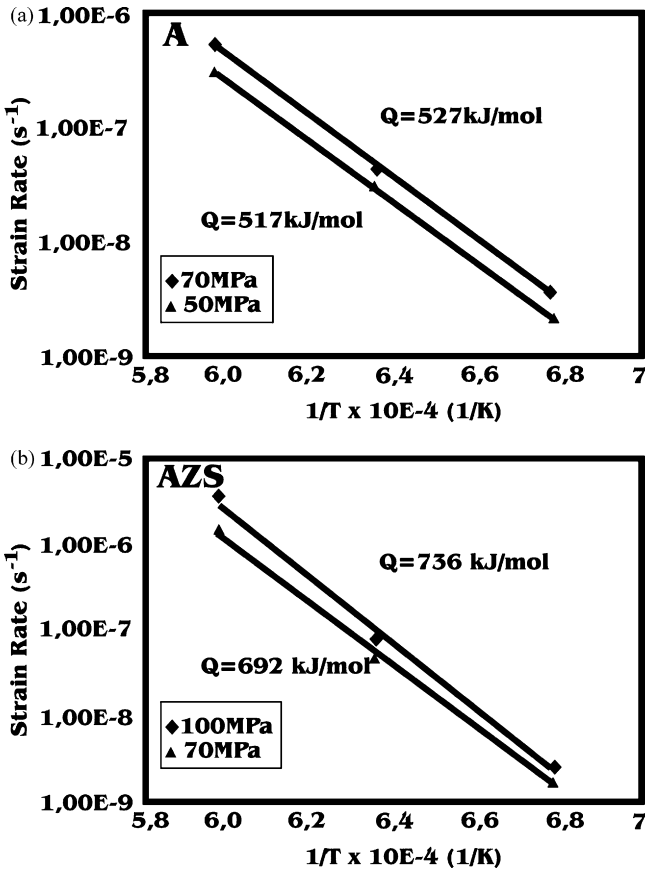

Fig. 8. Steady-state creep rate vs. reciprocal of the absolute temperature for: (a) A and (b) AZS.

Both regions can be clearly separated by a straight line for both materials, A and AZS. This line is given by pairs of critical stress and the corresponding critical strain rate for the temperatures 1200, 1300 and 1400 °C, respectively. For A this slow crack growth region can be defined by the following values: 1200 °C, 100 MPa; 1300 °C, 80 MPa; 1400 °C, 70 MPa and their corresponding strain rates. Between these three points a straight line can be drawn in the log strain rate–log applied stress, marking clearly the slow crack growth region of A. For AZS, the slow crack growth region can be defined by the following values: 1200 °C, 200 MPa; 1300 °C, 150 MPa; 1400 °C, 120 MPa and their corresponding strain rates. For this material a straight line can be drawn between these three points also, clearly separating the slow crack growth region for AZS. Fig. 6 shows clearly that the slow crack region is shifted nearly twice concerning the applied stresses in the considered temperature range 1200–1400 °C.

The calculated activation energies for A were 517 and 527 kJ/mol for an applied stress of 50 and 70 MPa, respectively (Fig. 8(a and b)). The activation energy for Al^{3+} grain boundary diffusion is 420 kJ/mol, whereas for Al^{3+} lattice diffusion the activation energy is 578 kJ/mol.[11–14] Comparing these values with the measured values, it is supposed that both, Al^{3+} grain boundary diffusion and Al^{3+} lattice diffusion are active in the measured temperature range 1200–1400 °C. Cannon and Coble[14] obtained a similar result for Mg-doped Al_2O_3 with grain sizes in the range 1–15 μm, suggesting cation boundary control for the fine-grained material and cation lattice control for the larger grained materials, but with a contribution of boundary diffusion, especially at lower temperatures. Taking into account that the measured grain size of A was 5.9 μm and the temperature range was 1200–1400 °C, the results from this study agree with these researchers and thus a combination of grain boundary diffusion controlled creep and lattice diffusion controlled creep is supposed to be the dominant creep mechanism for A. The measured stress exponent of 1.5 at 1200 and 1300 °C for A confirms this supposition. The calculated activation energies for AZS were 692 and 736 kJ/mol for an applied stress of 70 and 100 MPa, respectively (Fig. 8(a and b)). These values agree with the activation energies measured for Zr-doped Al_2O_3 in the literature. Wakai et al.[15,16] measured activation energies of 670 kJ/mol for 100 ppm zirconium-doped Al_2O_3, 760 kJ/mol for 1000 ppm zirconium-doped Al_2O_3 and 750 kJ/mol for alumina containing 20 wt% zirconia with an applied stress of 15 MPa at the temperature range 1250–1400 °C. Li et al.[8] reported 690 kJ/mol for 100 ppm zirconium-doped Al_2O_3 with an applied stress of 50 MPa at the temperature range 1250–1400 °C. Xue and Chen[17] obtained 728 kJ/mol for their 3 mol% ZrO_2-added alumina with an applied stress of 40 MPa at the temperature range 1200–1350 °C. Chevalier et al.[19] measured an activation energy of 760 kJ/mol for their Al_2O_3–10 vol% ZrO_2 composite. Flacher et al.[20,21] determined the activation energy being about

700 kJ/mol for alumina with the additions of 5, 10 and 20 vol% of zirconia. Clarisse et al.[22] examined the creep behaviour of a alumina–20 vol% zirconia composite and reported an activation energy of 715 kJ/mol for an applied stress of 30 MPa and 663 kJ/mol for an applied stress of 125 MPa at the temperature range 1275–1400 °C. Yoshida et al.[28] measured an activation energy of 650 kJ/mol for 0.1 wt% ZrO_2-doped Al_2O_3 and 700 kJ/mol for the composite Al_2O_3–10 wt% ZrO_2 (2.5 mol% Y_2O_3) at the temperature range 1250–1400 °C for an applied stress of 30 MPa. If these literature values are compared with the obtained results in the present work, we can conclude that the creep mechanism at the temperature interval 1200–1400 °C is grain boundary sliding accommodated by grain boundary diffusion, whereas at temperatures below 1200 °C accommodated lattice diffusion is the controlling mechanism.

The differences observed in creep behaviour of AZS nanocomposite and A can be explained as follows. A combination of grain boundary diffusion controlled creep and lattice diffusion controlled creep is supposed to be the dominant creep mechanism of alumina. When mullite particles are formed at alumina grain boundaries during sintering, compressive residual stresses are introduced on the mullite particles due to the expansive formation of mullite via a dissolution–precipitation mechanism. During cooling these compressive residual stresses are reinforced because mullite has the lowest thermal expansion coefficient of the three phases: alumina, tetragonal zirconia and mullite. Subsequent heating up to 1200 °C removes only a part of the introduced residual compressive stresses and thus sliding of alumina grains will be only possible if mullite nanoparticles are deformed. The high activation energy necessary to deform these mullite nanoparticles as well as the strong influence that nanosizes have on all thermally activated mechanisms (no defects present in nanoparticles) is very well known. As a consequence lattice diffusion controlled creep will be the dominant creep mechanism for AZS at 1200 °C. At higher temperatures the compressive stresses on mullite particles are completely removed and now the tetragonal zirconia particles are under compressive stresses. Thus, the dominant creep mechanism is grain boundary sliding accommodated by grain boundary diffusion.

In Fig. 8(a and b) it can be seen that at 1200 °C the strain rate of AZS is lower than the corresponding to A, at 1300 °C both samples have similar strain rates and at 1400 °C the strain rate of AZS is higher than the one corresponding to A. In order to compare these results, the differences in grain sizes of both materials have to be considered.

For lattice diffusion controlled creep, the grain size exponent p is 2 and for grain boundary diffusion controlled creep the grain size exponent is 3.[29–31] The creep rates of the sample AZS have been normalised with the grain size exponent 2, assuming that the dominant creep mechanism for AZS is lattice diffusion (Nabarro–Herring). Thus, a normalised strain rate for AZS $\dot{\varepsilon}_{nAZS}$ can be defined, taking into account the differences in grain sizes for A and AZS:

$$\dot{\varepsilon}_{nAZS} = \left(\frac{1}{d_A/d_{AZS}}\right)^p \dot{\varepsilon}_{AZS}, \quad (5)$$

where $\dot{\varepsilon}_{nAZS}$ is the measured creep rate for AZS, d_A the mean grain size of alumina and d_{AZS} is the mean grain size of AZS. With a mean grain size of 5.9 μm for A and 1.88 μm for AZS the normalised strain rate for AZS is calculated. The results of this normalisation for a grain size exponent of 2 are shown in Fig. 9. It can be observed that the strain rate of A is lowered by approximately two orders of magnitude.

Summarizing, it is supposed that the creep behaviour of AZS is controlled by the small quantity of tetragonal zirconia and mullite nanoparticles located at grain boundaries of alumina. The calculated stress exponents and the activation energy lead to the supposition that the dominant creep mechanism for AZS is lattice diffusion (Nabarro–Herring) at temperatures lower than 1200 °C and grain boundary sliding accommodated by grain boundary diffusion in the temperature range 1200–1400 °C. It is assumed that this behaviour is affected by the thermal stresses introduced during sintering due to the very expansive formation of mullite particles via a dissolution–precipitation mechanism.[1] The compressive residual stresses on the mullite particles are increased during cooling due to the different thermal expansion coefficients of alumina, tetragonal zirconia and mullite. It is believed that during the subsequent heating up to 1200 °C these compressive residual stresses are partly relaxed, but are still present and thus the dominating creep mechanism is lattice diffusion (Nabarro–Herring). At 1300 °C they are completely relaxed and the dominant creep mechanism is grain boundary sliding accommodated by grain boundary diffusion.

The slow crack growth region for both materials is limited by a maximum stress and the corresponding strain rate for the temperatures 1200, 1300 and 1400 °C. The creep region can be characterised by uniform values of stress exponent, activation energy and low strain rates, while the slow crack growth region is characterised by slow crack growth and finally catastrophic failure in a brittle manner. To avoid the risk of catastrophic failure of A and AZS at high temperatures, the range of stresses and temperatures at which deformation occurs by accommodated creep and not by creep damage or slow crack growth has to be determined. For A this slow crack growth region can be defined by the following values: 1200 °C, 100 MPa; 1300 °C, 80 MPa; 1400 °C, 70 MPa, whereas for AZS the following values were determined: 1200 °C, 200 MPa; 1300 °C, 150 MPa;

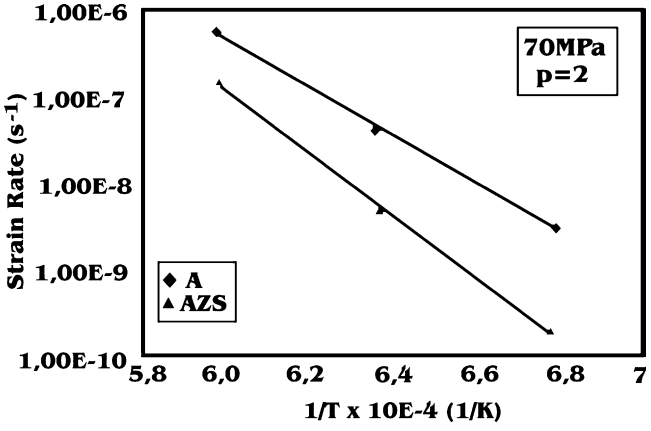

Fig. 9. Normalised creep rates with $p = 2$ for A and AZS.

1400 °C, 120 MPa. This means that the slow crack growth region is shifted nearly twice concerning the applied stress for the considered temperature range 1200–1400 °C. These differences can be explained taking into account the phase evolution of AZS during sintering[1] and the thermal expansion coefficients of alumina, tetragonal zirconia and mullite. Apart from alumina, no crystalline phase is observed up to 1000 °C. At this temperature the crystallisation of tetragonal zirconia begins and at 1550 °C mullite is formed. The formation of mullite through a transitory glassy phase is related with a high volume increase. The differential shrinkage curve of AZS confirmed this result because a sudden increase of the densification rate of AZS is observed for the temperature range 1580–1630 °C.[1] It is believed that this volume increase due to the formation of mullite introduces stresses at alumina grain boundaries. During cooling these introduced stresses increase due to the differences of the thermal expansion coefficients of alumina with $\alpha_{Al_2O_3} = 9.0 \times 10^{-6}\,K^{-1}$,[24,25] mullite with $\alpha_{Mullite} = 5.1 \times 10^{-6}\,K^{-1}$[26] and tetragonal zirconia with $\alpha_{t\text{-}ZrO_2} = 16 \times 10^{-6}\,K^{-1}$.[27] These differences cause the increase of the residual compression stresses of the mullite particles at room temperature. During heating up to 1200 °C, part of these stresses is removed due to the differences of thermal expansion coefficients mentioned before, but now acting in an inverse manner. The stresses are not removed completely so that the mullite particles are responsible for the creep behaviour of AZS at 1200 °C. This is reflected in a stress exponent of 1.2 and in a higher threshold stress for the appearance of slow crack growth. At 1300 °C the compressive stresses on mullite particles are completely removed and now the tetragonal zirconia particles are under compressive stresses. As a consequence, they are responsible for the creep and slow crack growth behaviour at 1300 °C.

The introduced stresses at alumina grain boundaries and the very homogenous microstructure of AZS are considered to be responsible for the dramatic improvement of the safety working conditions of alumina. The line separating the slow crack growth region and the creep region is shifted nearly twice concerning the applied stresses at the considered temperature range 1200–1400 °C.

4. Conclusions

The colloidal processing route used in this study leads to a very homogeneous microstructure with tetragonal zirconia and mullite nanoparticles located at nearly 100% of all triple points and alumina grain boundaries. Tetragonal zirconia and mullite nanoparticles are formed during sintering at alumina grain boundaries. The formation of mullite through a transitory glassy phase via a dissolution–precipitation mechanism is related to a high volume increase and, as a consequence, a homogenous residual stress field is introduced at grain boundaries.

The presence of these zirconia and mullite nanoparticles changes completely the deformation mechanisms in this composite compared to those operating in pure alumina. At 1200 °C sliding of alumina grains is blocked by the presence of mullite nanoparticles because the compressive residual stresses introduced during sintering are not removed completely at 1200 °C. As a consequence, the creep mechanism operating at this temperature is lattice diffusion controlled creep. At higher temperatures the compressive stresses on mullite particles are completely removed and now the tetragonal zirconia particles are under compressive stresses. Thus, the dominant creep mechanism is grain boundary sliding accommodated by grain boundary diffusion. The homogenous residual stress field introduced during sintering due to the formation of mullite via a dissolution–precipitation mechanism and the change of the stress state during heating due to the different thermal expansion coefficients of alumina, tetragonal zirconia and mullite have a strong effect on the threshold for the appearance of slow crack growth at high temperatures. A dramatic improvement of the safety working conditions of alumina is achieved. The line in the logarithmic strain rate versus stress plot, separating the slow crack growth and the creep region, is shifted nearly twice concerning the applied stresses at the temperature range 1200–1400 °C.

Acknowledgements

The authors would like to acknowledge the EU financial support received under the GROWTH2000 project reference BIOKER G5RD-CT-2001-00483 and the support of the Spanish Ministry of Education and Science project reference MAT2003-04199-C02-01.

References

1. Schehl, M., Díaz, L. A. and Torrecillas, R., Alumina based nanocomposites from powder-alkoxide mixtures. *Acta Mater.*, 2002, **50**, 1125–1139.
2. Schehl, M., Díaz, L. A. and Torrecillas, R., Creep behaviour of alumina/YAG nanocomposites obtained by a colloidal processing route. *J. Eur. Ceram. Soc.*, 2007, **27**(1), 143–150.
3. Torrecillas, R., Moya, J. S., de Aza, S., Gros, H. and Fantozzi, G., Microstructure and mechanical properties of mullite–zirconia reaction-sintered composites. *Acta Metall. Mater.*, 1993, **41**(6), 1647–1652.
4. Jang, H. M., Cho, S. M. and Kim, K. T., Alumina–mullite–zirconia composites: part 1 colloidal processing and phase-formation characteristics. *J. Mater. Sci.*, 1996, **31**, 5083–5092.
5. Jang, H. M., Cho, S. M. and Kim, K. T., Alumina–mullite–zirconia composites: part 2 microstructural development and toughening. *J. Mater. Sci.*, 1997, **32**, 503–511.
6. Mazzei, A. C. and Rodrigues, J. A., Alumina–mullite–zirconia composites obtained by reaction sintering: part 1 microstructure and mechanical behaviour. *J. Mater. Sci.*, 2000, **35**, 2807–2814.
7. Mazzei, A. C., Rodrigues, J. A. and Pandolfelli, V. C., Alumina–mullite–zirconia composites obtained by reaction sintering: part 2 *R*-curve behaviour. *J. Mater. Sci.*, 2000, **35**, 2815–2824.
8. Li, Y. Z., Wang, C., Chan, H. M., Rickman, J. M., Harmer, M. P., Chabala, J. M. *et al.*, Codoping of alumina to enhance creep resistance. *J. Am. Ceram. Soc.*, 1999, **82**(6), 1497–1504.
9. Torrecillas, R., Calderón, J. M., Moya, J. S., Reece, M. J., Davies, C. K. L., Olagnon, C. *et al.*, Suitability of mullite for high temperature applications. *J. Eur. Ceram. Soc.*, 1999, **19**, 2519–2527.
10. Hollenberg, G. W., Terwellinger, G. R. and Gordon, R. S., Calculation of stresses and strains in four point bending creep tests. *J. Am. Ceram. Soc.*, 1971, **54**(4), 196–199.
11. Cannon, R. M., Rhodes, W. H. and Heuer, A. H., Plastic deformation of fine-grained alumina (Al_2O_3): I interface-controlled diffusional creep. *J. Am. Ceram. Soc.*, 1980, **63**(1/2), 46–53.

12. Heuer, A. H., Tighe, N. J. and Cannon, R. M., Plastic deformation of fine-grained alumina (Al_2O_3): II basal slip and nonaccommodated grain boundary sliding. *J. Am. Ceram. Soc.*, 1980, **63**(1/2), 53–58.
13. Chokshi, A. H. and Porter, J. R., High temperature mechanical properties of single phase alumina. *J. Mater. Sci.*, 1986, **21**, 705–710.
14. Cannon, R. M. and Coble, R. L., Review of diffusional creep of Al_2O_3. In *Deformation of Ceramic Materials*, *Vols. 61–100*, ed. R. C. Bradt and R. E. Tressler. Plenum Press, New York, 1975.
15. Wakai, F., Iga, T. and Nagano, T., Effect of dispersion of ZrO_2 particles on creep of fine-grained Al_2O_3. *J. Jpn. Ceram. Soc.*, 1988, **96**(12), 1206–1209.
16. Wakai, F., Nagano, T. and Iga, T., Hardening in creep of alumina by zirconium segregation at the grain boundary. *J. Am. Ceram. Soc.*, 1997, **80**(9), 2361–2366.
17. Xue, L. A. and Chen, I. W., Superplastic alumina at temperatures below 1300 °C using charge-compensating dopants. *J. Am. Ceram. Soc.*, 1996, **79**(1), 233–238.
18. Calderón-Moreno, J. M., de Arellano-López, A. R., Dominguez-Rodriguez, A. and Routbort, J. L., Microstructure and creep properties of alumina–zirconia ceramics. *J. Eur. Ceram. Soc.*, 1995, **15**, 983–988.
19. Chevalier, J., Olagnon, C., Fantozzi, G. and Gros, H., Creep behaviour of alumina, zirconia and zirconia-toughened alumina. *J. Eur. Ceram. Soc.*, 1997, **17**, 859–864.
20. Flacher, O., Blandin, J. J. and Plucknett, K. P., Effects of zirconia additions on the superplasticity of alumina–zirconia composites. *Mater. Sci. Eng.*, 1996, **221A**, 102–112.
21. Flacher, O., Blandin, J. J., Plucknett, K. P., Wilkinson, D. S. and Caceres, C. H., Effects of porosity on the superplastic properties of submicronic alumina–zirconia composites. *Mater. Sci. Forum*, 1997, **243–245**, 411–416.
22. Clarisse, L., Baddi, R., Bataille, A., Crampon, J., Duclos, R. and Vicens, J., Superplastic deformation mechanisms during creep of alumina–zirconia composites. *Acta Mater.*, 1997, **45**(9), 3843–3853.
23. Okada, K. and Sakuma, T., Tensile ductility in zirconia-dispersed alumina at high temperatures. *J. Am. Ceram. Soc.*, 1996, **79**(2), 499–502.
24. Bayer, G., Thermal expansion anisotropy of oxide compounds. *Proc. Br. Ceram. Soc.*, 1973, **22**, 39.
25. Salem, J. A., Li, Z. and Bradt, R. C., Thermal expansion and elastic anisotropy in single crystal Al_2O_3 and SiC whiskers. In *Proceedings Symposium on Advances in Composite Material and Structures*, 1986.
26. Bartolomé, J. F., Moya, J. S., Llorca, J. and Anglada, M., Fatigue crack growth behaviour in mullite/alumina functionally graded ceramics. *J. Am. Ceram. Soc.*, 1998, **81**(6), 1502–1508.
27. Patil, R. N. and Subbarao, E. C., Axial thermal expansion of ZrO_2 and HfO_2 in the range room temperature to 1400 °C. *J. Appl. Crystallogr.*, 1969, **2**(Pt. 6), 281–288.
28. Yoshida, H., Ikuhara, Y. and Sakuma, T., A critical factor to determine the high-temperature creep resistance in cation-doped polycrystalline Al_2O_3. *Key Eng. Mater.*, 2000, **171–174**, 809–816.
29. Nabarro, F. R. N., Steady state diffusional creep. *Philos. Mag.*, 1967, **16**, 231–237.
30. Herring, C., Diffusional viscosity of a polycrystalline solid. *J. Appl. Phys.*, 1950, **21**(5), 437–445.
31. Coble, R. L., A model for boundary diffusion controlled creep in polycrystalline materials. *J. Appl. Phys.*, 1963, **34**(6), 1679–1682.